Neutral recycling effects on ITG turbulence

2017 Nucl. Fusion 57 086028

(http://iopscience.iop.org/0029-5515/57/8/086028)

IOP Publishing | International Atomic Energy Agency Nuclear Fusion

Nucl. Fusion **57** (2017) 086028 (7pp) https://doi.org/10.1088/1741-4326/aa7807

Neutral recycling effects on ITG turbulence

D.P. Stotler, J. Lang[1], C.S. Chang, R.M. Churchill and S. Ku

Princeton Plasma Physics Laboratory, Princeton University, Princeton, NJ 08543-451, United States of America
[1] Intel Corporation, Santa Clara, CA, United States of America

E-mail: dstotler@pppl.gov

Received 15 December 2016, revised 11 May 2017
Accepted for publication 8 June 2017
Published 4 July 2017

Abstract

The effects of recycled neutral atoms on tokamak ion temperature gradient (ITG) driven turbulence have been investigated in a steep edge pedestal, magnetic separatrix configuration, with the full-*f* edge gyrokinetic code XGC1. An adiabatic electron model has been used; hence, the impacts of neutral particles and turbulence on the density gradient are not considered, nor are electromagnetic turbulence effects. The neutral atoms enhance the ITG turbulence, first, by increasing the ion temperature gradient in the pedestal via the cooling effects of charge exchange and, second, by a relative reduction in the $E \times B$ shearing rate.

Keywords: gyrokinetic simulation, plasma turbulence, neutral recycling, tokamak, FEC 2016

(Some figures may appear in colour only in the online journal)

1. Introduction

ITER and other future burning plasma devices are expected to operate in the high confinement mode, or H-mode. Yet, the means by which a tokamak initially in the low confinement regime (L-mode) transitions into H-mode (L-H) is not well understood, nor are the mechanisms that suppress the turbulence and maintain the steep gradients in the H-mode. Although the effects of neutral particles (e.g. due to recycling) on core plasma fueling are more frequently discussed, their impact on plasma turbulence, the L-H transition, and H-mode remain open areas of investigation, theoretically [1, 2] and experimentally [3, 4]. For example, the role of neutral atoms in the processes that set the L-H threshold power has been the focus of multiple theoretical models [5–9]. That neutrals affect the L-H transition has also been demonstrated experimentally [10–14]. The momentum and energy losses associated with neutral-ion interaction have been quantified [15, 16]. However, direct numerical simulation of the effects of neutrals on plasma instabilities and turbulence has previously been impractical due to the associated computational and algorithmic challenges.

The most relevant plasma-atom interactions are electron impact ionization and resonant charge exchange (CX). Hydrogen molecules released from plasma facing surfaces by various plasma interaction processes, referred to collectively as 'recycling', are dissociated and/or ionized close to the walls; only the relatively energetic product atoms ($\sim$3 eV) have mean free paths long enough to penetrate inside closed flux surfaces. Because such atoms are inevitably migrating into a region with hotter ions, subsequent CX interactions have a cooling effect on the ion distribution. Moreover, the finite widths of the ion banana orbits cause this cooling to be felt beyond the location of the CX collision. The increased energies of the resulting atoms lead to even longer mean free paths and, thus, deeper penetration into the confined plasma [17]. Note that the eventual ionization of these atoms represents a local power source for the ions, offsetting some of the charge exchange cooling [16]. The multistep excitation, de-excitation, radiative decay, and ionization processes contributing to the collisional radiative 'ionization' of a particular atom [18] also represent a significant power sink for the electron population, although it is not considered in this investigation. Electron-ion recombination can be a significant or even dominant process in high density, low temperature ($<$1 eV) divertor plasmas, but is of little relevance to instabilities in the edge plasma.

One obvious consequence of the pedestal CX cooling is a steepening of the ion temperature profile and an associated enhancement in gradient driven instabilities and turbulence. However, neutrals can also impact the $E \times B$ shear flows that are critical in determining the potency of turbulent fluctuations [2, 6]. In this paper, we use the full-*f*, gyrokinetic, particle-in-cell code XGC1 [19–22], with its adiabatic electron option, to

investigate how all of the modeled processes impact ion temperature gradient (ITG) driven turbulence. The use of the adiabatic electron model enables us to carry out this study without employing extreme scale computing resources. However, this restriction does not allow us to examine the interplay of neutral particle effects with the particle flux, density gradient, and electromagnetic turbulence, all important in pedestal confinement [23–27]. Kinetic electron and electromagnetic effects will be examined as part of our future research.

Essential to this investigation is XGC1's ability to simulate the entire plasma from the magnetic axis to the material walls in a realistic separatrix geometry, typically specified via a numerical equilibrium in the EFIT EQDSK format [28]. The boundary conditions at the material surfaces intersected by open field lines are set via a logical sheath criterion [29] in a typical XGC1 simulation. However, with the adiabatic electron model used in these simulations, the plasma potential is set to zero in the entire scrape-off layer (SOL). This simplifying assumption is not expected to affect our results given that penetration of the ITG turbulence into the SOL is weak due to the parallel connection with the conducting wall via ion sound waves [22]. Neutral particles resulting from the subsequent plasma-material interaction are consistently simulated with a built-in Monte Carlo procedure, described below. Charged particle collisions are effected by a nonlinear Fokker-Planck-Landau collision operator [30, 31]. XGC1 also allows the specification of additional heat, momentum, and particle sources (e.g. neutral beam injection).

The neutral transport model used by XGC1 is described in section 2. The simulations, one without recycling, as if the walls were purely absorbing, and one with an experimentally relevant 99% recycling, are described in section 3. The effects of the assumed recycling model on the plasma profiles and turbulence are examined in that same section. Our conclusions are presented in section 4.

2. Neutral transport model

Two neutral transport models are available within the XGC code family. The most sophisticated is accessed via a subroutine interface to the DEGAS2 Monte Carlo neutral transport code [32, 33]. The other traces back to the built-in routine in the original, full-*f*, *drift-kinetic*, neoclassical XGC0 code [19], to which improvements have been made [34]. The former allows the incorporation of detailed models for plasma-material interactions and additional neutral species, e.g. molecules. Given the focus of the present work on the confined plasma, that added complexity is superfluous, and the built-in model, which treats only atoms, will suffice. We demonstrate this quantitatively in section 3 via the integrated CX cooling rate, the physical quantity most pertinent to this investigation.

Both models utilize a 'test particle' Monte Carlo approach for dealing with the nonlinearity of the neutral-plasma collision operator [33] that involves two complementary plasma-neutral collision routines. In the first, kinetic neutrals collide off a fluid plasma background obtained from the kinetic particle information, yielding 2-D profiles for the neutral density, temperature, and flow velocity. In the second, the kinetic plasma species collide with this neutral fluid background, altering the plasma particle distribution functions in the process.

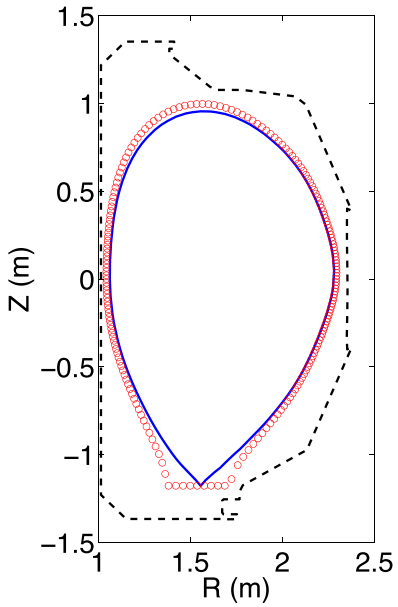

Figure 1. The dashed lines represent the simulation boundary, determined from the geometry of the DIII-D vacuum vessel. The blue line is the plasma separatrix as specified in the EFIT equilibrium for shot 096333. The red circles delineate the corresponding neutral birth surface.

The effects of the molecules are implicitly incorporated into the built-in kinetic neutral routine by establishing a neutral birth surface in the SOL a finite distance from the vacuum vessel walls (figure 1) and launching there atoms with a 3 eV, thermal, isotropic distribution, as if they had been produced by molecular dissociation. For the purposes of this study, we specify a spatial distribution for the neutral flux that is peaked around the X-point, as one would expect in a discharge dominated by divertor recycling. Specifically, this distribution is

$$\Gamma = \Gamma_0 \left[1 + 9\exp(-\Delta\theta^2/\Delta\theta_0^2)\right], \tag{1}$$

where the $\Delta\theta$ represents the difference in poloidal angle, measured relative to the magnetic axis-midplane line, between the birth point and the X-point. The width $\Delta\theta_0$ is taken to be $\pi/6$, as in [19], to cover the full extent of the divertor plates and account for neutral diffusion. The results are insensitive to the value of $\Delta\theta_0$, provided that it is not too small.

The atoms are then tracked through the plasma, undergoing ionization and charge exchange along the way. That background plasma is characterized by a Maxwellian distribution, the parameters of which are determined from the current state of the XGC1 (kinetic) plasma. The neutral fluid moments are updated along the tracks.

The ionization rate is specified via the fit:

$$S_{\rm ion} = 8\times10^{-15}\frac{\sqrt{T_{\rm e}}\,\exp(-13.56/T_{\rm e})}{(1.0+0.01T_{\rm e})}\ {\rm m}^3\,{\rm s}^{-1}, \tag{2}$$

where $T_{\rm e}$ is the electron temperature in eV. For $10 < T_{\rm e} < 10^3$ eV and $n_{\rm e} < 10^{19}\,{\rm m}^{-3}$, the deviation from a full collisional-radiative

result [17] is <20%; it's uniformly larger for higher densities. The fit used for the CX rate is:

$$S_{cx} = 1.1 \times 10^{-14}(E_i^{0.3}/\sqrt{M_i})\ \mathrm{m^3\ s^{-1}}, \quad (3)$$

where E_i is the ion energy or temperature in eV, depending on the application, and M_i is the ion mass in AMU. The deviation from a comprehensive value for the rate, e.g. as in [35], is <5% for all atom energies at $T_i = 100$ eV. Generally, the discrepancy is larger for smaller T_i or larger energies, but is only 13% at $T_i = 1$ eV and 3 eV atom energy.

The overall magnitude of the neutral density used in the 'kinetic plasma' neutral-plasma collision routine is set so that the volume integrated ionization rate divided by the loss rate of ions to the material surfaces equals the user-specified recycling rate, effectively determining Γ_0 in equation (1). In our simulation with neutral recycling, this recycling rate is 99%. The same rate expressions, equations (2) and (3), are used in this routine. The new ions produced by these reactions are sampled from the neutral distribution.

3. Effects on ITG turbulence

The two simulations documented here are based on a model equilibrium for the DIII-D H-mode shot 96333 [36]. A continuous heating source of 2 MW, consistent with the experimental neutral beam injection rate, is applied in the core region; the associated torque source is neglected. No impurity species are included.

The initial density and ion temperature profiles, figure 2, are specified via analytic expressions calibrated to resemble the profiles used in the EFIT equilibrium calculation. The density pedestal is about 10 ion gyroradii (evaluated at the pedestal top) wide. Detailed edge plasma data are not available in this case for both electron and ion temperatures; we make the experimentally relevant assumption that the fixed T_e pedestal is steeper than that of T_i. Note that the T_i plotted in figure 2 is actually $\frac{2}{3}\langle E\rangle$, where $\langle E\rangle$ is the average over the distribution function of the total particle kinetic energy; it will differ somewhat from the usual Maxwellian temperature unless the particle distribution function is Maxwellian and net flow is negligible. The full-*f* XGC1 code quickly evolves the ion temperature and density profiles to a gyrokinetic equilibrium consistent with the specified sources/sinks, ITG and neoclassical transport, and the magnetic field [22]. Given the present focus on ITG turbulence, with the electrons treated adiabatically, the turbulence does not drive any particle transport; the only changes in the ion density profile (and, thus, in the quasi-neutral electron density profile) arise from the sources and sinks. That is, the difference between the dashed and solid lines in figure 2(*a*) represents the ionization particle source of the penetrating neutral atoms, minus the particle sinks due to parallel ion loss to the divertor plate and X-point orbit loss. As is apparent in figure 2, the modification of the density pedestal shape by neutral ionization, in the brief time interval simulated, is slow and small compared with the changes to T_i; the time variation of η_i is interpreted as being mostly due to the latter. A more in-depth examination of density profile effects

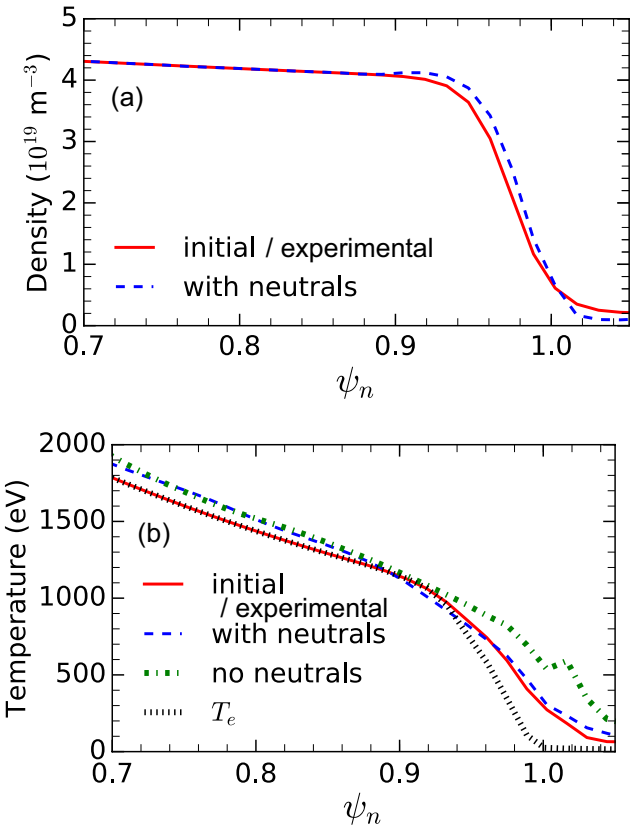

Figure 2. (*a*) Initial and final ion density profiles in the with-neutrals run, showing the effects of the neutral ionization source. In the no-neutrals case, the ion density profile remains the same as the initial one. (*b*) Initial and final ion temperature profiles, along with the (fixed) electron temperature profile.

will require the kinetic electron and electromagnetic options in XGC1. Again, the electron temperature profile is held fixed here.

Before examining the turbulence, we use these profiles to compare the plasma-neutral energy exchange rates obtained from the built-in neutral transport model with those provided by a comprehensive DEGAS2 simulation, giving an estimate of the uncertainty introduced by the various approximations made within the former. To assemble the input required for DEGAS2, we exploit the existing coupling between the drift-kinetic, neoclassical XGC0 plasma transport code and DEGAS2 (details on XGC0, DEGAS2, and their coupling can be found in [33]), initializing XGC0 with the same magnetic equilibrium and input plasma profiles as XGC1 and allowing it to map those profiles onto a triangular mesh common to both XGC0 and DEGAS2. The variation of the D_2 source flux along the mesh boundary is computed from equation (1). DEGAS2 is then run in time independent mode. As the molecules penetrate the plasma, they undergo ionization and dissociation; resulting molecular ions are assumed to be ionized, dissociated, or recombined immediately. Any product atoms are then tracked through the plasma and interact with it via ionization and charge exchange. The rates used for these processes are as in [17] and references therein. The particle track terminates upon ionization of the atom.

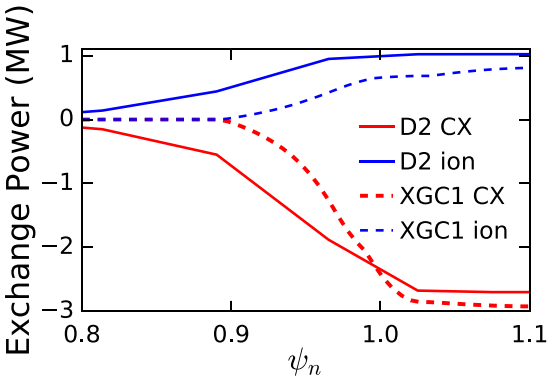

Figure 3. Cumulative integrated power provided to the ions by neutral charge exchange (red curves) and ionization (blue) as a function of the normalized poloidal flux for both DEGAS2 (solid curves) and XGC1's built-in neutral transport model (dashed). These calculations were performed with the initial plasma profiles. Note that the XGC1 neutral transport model is not run for $\psi_n < 0.9$ so that the neutral density is set to zero in that volume.

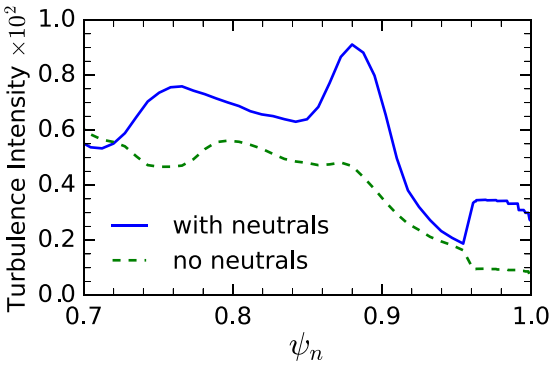

Figure 4. Turbulence intensity $e\sqrt{\langle\delta\phi^2\rangle}/T_e$ in the two runs.

The neutral-plasma mass and energy exchange rate data are reduced to functions of the normalized poloidal flux to facilitate comparison. In the DEGAS2 mesh, the triangles inside the separatrix are distributed over the annular volumes defined by a selected set of flux surfaces. This allows volumetric quantities, such as these exchange rates, to be easily integrated in the poloidal direction. In particular, we can use them to determine the total ionization rate inside the separatrix, $S_{\mathrm{ion,D2}}$. The corresponding data from XGC1's neutral transport model are compiled as a function of flux surface directly from the particle locations; we designate the integral of the ionization rate over the volume inside the separatrix as $S_{\mathrm{ion,XGC1}}$. The two models' characterizations of the neutral source and physics in the volume outside the separatrix differ fundamentally. Yet, as noted in section 2, these differences are much less relevant to the present work than the ionization and charge exchange processes that dominate the neutral behavior inside the separatrix. To allow us to compare the models' treatment of the latter on an equal footing, we scale the DEGAS2 results by $S_{\mathrm{ion,XGC1}}/S_{\mathrm{ion,D2}}$. The cumulative energy exchange rates are then plotted as a function of normalized poloidal flux in figure 3. The total CX cooling rates for the two models differ by only 17%, and those for ionization by 24%. Note that the latter represents the energy of newly created ions; electron cooling is not considered here. Differences of this magnitude are minor in comparison with the other uncertainties in the tokamak plasma model, such as the characterization of plasma-material interactions.

The net cooling of ∼2 MW in figure 3 pertains only to these initial profiles. This value drops rapidly as the simulation evolves due to transport and gyrokinetic relaxation to a quasi-equilibrium. In particular, the integrated CX cooling rate is ∼0.8 MW at $t = 3.9$ ms.

The 99% recycling simulation ('with-neutrals') is run until the plasma profiles and turbulence self-organize into a quasi-steady state, about 4 ms real time. This state is defined as that in which the relative changes in the plasma and turbulence profiles during a toroidal ion bounce, collision, and turbulence correlation time (all <0.5 ms) are less than the simulation error [21]. Achieving a perfect steady state is not possible in this short-time gyrokinetic simulation since the plasma is evolving on a global transport time scale due to imperfect balances between the sources and sinks, e.g. the less than unity recycling. In the corresponding simulation without recycling ('no-neutrals'), run for 3.4 ms, the ion temperature profile is still evolving at the end, and the SOL density is being depleted due to particle losses to the walls that are not being replenished by neutral ionization.

The general properties of the turbulence are similar to those described in [22] and are not discussed here. As is typical, the energy cascade to longer wavelengths transfers the turbulence energy from the wavenumbers associated with the maximum linear growth rate ($k_\theta \rho_i \sim 0.3 - 0.4$, as is shown in figure 7 of [21]).

The flux surface averaged turbulence intensity in the two runs is quantified by $e\sqrt{\langle\delta\phi^2\rangle}/T_e$, with $\sqrt{\langle\delta\phi^2\rangle}$ being the RMS average over the flux surface of the deviation of the electrostatic potential from its toroidal mean. Since the profiles of this quantity fluctuate in time, we plot in figure 4 an average over a 400 time step interval (∼0.6 ms). As can seen in this comparison, the saturated turbulence level in the with-neutrals run is the larger of the two. The linear drive for ITG exists at the top of the density pedestal ($\psi_n < 0.92$) where the ion temperature gradient is finite and the density gradient is small, not where the density profile is steep. The turbulence in the latter region is the result of non-local spreading.

The temporal evolution of the ion temperature profiles (figure 2) provides some insight into the origin of this difference in turbulence intensity. The ion temperature gradients for $\psi_n \equiv \psi/\psi_{\mathrm{sep}} = 0.85 \rightarrow 1$ in the with-neutrals case are larger than in the no-neutrals run. The profile for the former has saturated to a state that differs only modestly from the initial one, while the latter has increased and flattened substantially. Since the only difference between the two simulations is the neutral recycling model, we infer that these effects are associated with the effective ion cooling associated with charge exchange. Note that these effects propagate further into the core than the neutral penetration depth as a result of finite banana orbit mixing, as well as via neoclassical and turbulent transport.

To further quantify this effect, we compute the ITG turbulence drive [37]

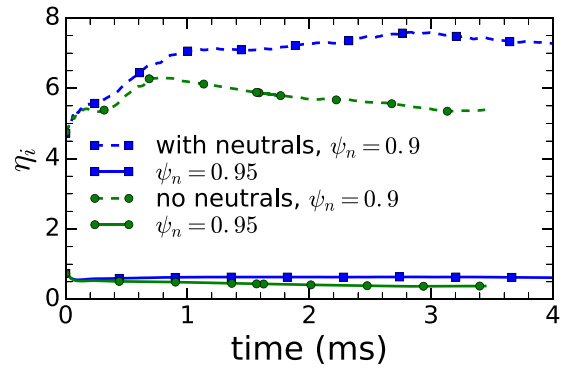

Figure 5. Temporal evolution of η_i at (*a*) $\psi_n = 0.9$ and (*b*) 0.95 in the two simulations.

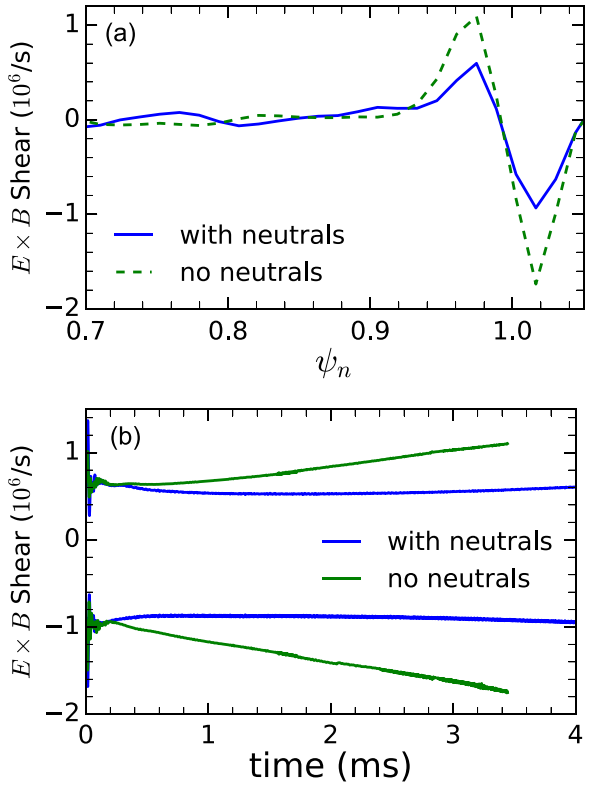

Figure 6. (*a*) Radial profiles of $E \times B$ shearing rate in the two simulations. (*b*) Temporal evolution of the maximum and minimum values in (*a*). The profiles in (*a*) were taken at 3.9 ms (3.4 ms) in the with-neutrals (no-neutrals) run.

$$\eta_i \approx (\mathrm{d} \ln T_i/\mathrm{d}\psi)/(\mathrm{d} \ln n_{e0}/\mathrm{d}\psi), \quad (4)$$

where n_{e0} is the initial electron density (figure 5). Throughout the runs, the with-neutrals η_i values in the region of interest, $0.85 < \psi_n < 1$, are larger than those in the no-neutrals case. Moreover, the latter are falling uniformly, consistent with a turbulence intensity that is steadily decreasing in time.

A second factor contributing to the differences noted in figure 4 is that the $E \times B$ shearing rate $\mathrm{d}v_{E\times B}/\mathrm{d}R$ in the steep gradient region is significantly larger in the no-neutrals case (figure 6(*a*)), consistent with the reduced turbulence intensity in that run [22]. The temporal evolution of the maximum and minimum shear values in the two runs (figure 6(*b*)) parallels that of η_i. Namely, with neutrals, the shear is steady through all but the earliest stages of the run, and trending uniformly towards increased shear for the no-neutrals case as a result of the continuous flattening of the T_i profile. The latter leads to a progressive reduction in turbulence intensity; the turbulence does not achieve a steady state by the end of the no-neutrals simulation. The speed with which the turbulence spreads into the pedestal is estimated in [21] to be $\sim v_i\rho_i/R$, (with v_i and ρ_i being the ion thermal velocity and gyroradius, respectively, and R the plasma major radius). Crossing the $10\rho_i$ width of the pedestal at this speed requires $\sim$0.2 ms, consistent with the transient turbulence spreading time scale seen in these simulations.

Note that the effect of the charge-exchange-enhanced ion temperature gradient on the radial force balance is countered by a reduction in the magnitude of the negative ion parallel flow, in a way consistent with the charge exchange drag on the ion parallel flow, the $E \times B$ flow, and turbulence.

The connections between sheared $E \times B$, or zonal flows, and L-mode confinement, L-H transition, and internal transport barriers have been the subject of many investigations [38–40]. For example, a reduction in the zonal flow results in an increase in the L-H power threshold [41]. Analogous damping of the zonal flow rate by the charge exchange friction, and the associated increase in L-H transition power, has been predicted theoretically [5, 6]. The region of reduced $E \times B$ shear overlaps with the neutral penetration zone, suggesting that our result is consistent with those predictions.

4. Conclusions

We have shown that the neutral atoms generated by recycling enhance ITG turbulence through an increase in the ion temperature gradient and a relative reduction in the $E \times B$ shearing rate. Moreover, our results imply that the neutral recycling rate is a relevant parameter in determining pedestal confinement. The mean free paths of $\gtrsim$3 eV neutral atoms, such as those produced by molecular dissociation and subsequent charge exchange, are long enough to reach at least the lower part of the H-mode pedestal. The ensuing ionization and charge exchange reactions alter the ion distribution function there. This, in turn, impacts the ITG turbulence non-locally through neoclassical banana excursion and nonlocal turbulence interactions. Only with a full-f gyrokinetic simulations, such as that provided by XGC1, can these neoclassical, neutral, and turbulence effects be rendered consistently.

Actual comparison of these results with experimental observations to be done in the future will require even more complete simulations. For example, the use of kinetic electrons will allow a consistent evolution of their temperature, as well as both density profiles. Treatment of electromagnetic turbulence will be required for meaningful comparisons with experimental observations and other predictions. The use of a comprehensive neutral transport model, e.g. via DEGAS 2, will provide a more accurate neutral source profile and allow molecular processes to be included.

Acknowledgments

This work is supported by US DOE Contract DE-AC02-09CH11466. Most of the support in this contract was provided through the Scientific Discovery through Advanced Computing (SciDAC) program funded by the US DOE Office of Advanced Scientific Computing Research and the Office of Fusion Energy Sciences. Awards of computer time were provided by the Innovative and Novel Computational Impact on Theory and Experiment (INCITE) program. This research used resources of the Oak Ridge Leadership Computing Facility, which is a DOE Office of Science User Facility supported under contract DE-AC05-00OR22725, as well as the National Energy Research Scientific Computing Center, a DOE Office of Science User Facility supported under Contract No. DE-AC02-05CH11231. The digital data for this paper can be found in http://arks.princeton.edu/ark:/88435/dsp018p58pg29j.

ORCID

D.P. Stotler https://orcid.org/0000-0001-5521-8718

References

[1] Fülöp T., Catto P.J. and Helander P. 2001 Effect of neutral atoms on tokamak edge plasmas *Phys. Plasmas* **8** 5214–20
[2] Fülöp T., Helander P. and Catto P.J. 2002 Effect of poloidal density variation of neutral atoms on the tokamak edge *Phys. Rev. Lett.* **89** 225003
[3] Maingi R. *et al* and The NSTX Team 2004 Effect of gas fuelling location on H-mode access in NSTX *Plasma Phys. Control. Fusion* **46** A305–13
[4] Cao B., Zweben S., Stotler D.P., Bell M., Diallo A., Kaye S.M. and LeBlanc B. 2012 Edge turbulence velocity changes with lithium coating on NSTX *Plasma Phys. Control. Fusion* **54** 112001
[5] Carreras B.A., Diamond P.H. and Vetoulis G. 1996 Role of neutrals in the phase transition model *Phys. Plasmas* **3** 4106–14
[6] Carreras B.A., Owen L.W., Maingi R. and Mioduszewski P.K. 1998 Effect of edge neutrals on the low-to-high confinement transition threshold in the DIII-D tokamak *Phys. Plasmas* **5** 2623–36
[7] Groebner R.J., Mahdavi M.A., Leonard A.W. and Osborne T.H. 2002 The role of neutrals in high-mode (H-mode) pedestal formation *Phys. Plasmas* **9** 2134–40
[8] D'Ippolito D.A. and Myra J.R. 2002 Effect of ion-neutral charge exchange on radial electric fields in the edge plasma *Phys. Plasmas* **9** 853–60
[9] Stacey W.M. 2002 Spontaneous edge transport barrier formation due to suppression of edge thermal instabilities as a lowhigh trigger mechanism in tokamaks *Phys. Plasmas* **9** 3082–8
[10] Owen L.W., Carreras B.A., Maingi R., Mioduszewski P.K., Carlstrom T.N. and Groebner R.J. 1998 Assessment of effects of neutrals on the power threshold for LH transitions in DIII-D *Plasma Phys. Control. Fusion* **40** 717–20
[11] Colchin R.J., Maingi R., Fenstermacher M.E., Carlstrom T.N., Isler R.C., Owen L.W. and Groebner R.J. 2000 Measurement of neutral density near the X point in the DIII-D tokamak *Nucl. Fusion* **40** 175–80
[12] Boivin R.L. *et al* 2000 Effects of neutral particles on edge dynamics in alcator C-mod plasmas *Phys. Plasmas* **7** 1919–26
[13] Friis Z.W., Stacey W.M., Leonard A.W. and Rensink M.E. 2010 Analysis of neutral particle recycling and pedestal fueling in a H-mode DIII-D discharge *Phys. Plasmas* **17** 022507
[14] Battaglia D.J. *et al* and The NSTX Team 2013 Dependence of the lh transition on x-point geometry and divertor recycling on NSTX *Nucl. Fusion* **53** 113032
[15] Versloot T.W. *et al* and JET-EFDA Contributors 2011 Momentum losses by charge exchange with neutral particles in H-mode discharges at JET *Plasma Phys. Control. Fusion* **53** 065017
[16] Zweben S.J. *et al* 2014 Effect of a deuterium gas puff on the edge plasma in NSTX *Plasma Phys. Control. Fusion* **56** 095010
[17] Stotler D.P., Scotti F., Bell R.E., Diallo A., LeBlanc B.P., Podesta M., Roquemore A.L. and Ross P.W. 2015 Midplane neutral density profiles in the National Spherical Torus Experiment *Phys. Plasmas* **22** 082506
[18] Johnson L.C. and Hinnov E. 1973 Ionization, recombination, and population of excited levels in hydrogen plasmas *J. Quant. Spectrosc. Radiat. Transfer* **13** 333–58
[19] Chang C.S., Seunghoe K. and Weitzner H. 2004 Numerical study of neoclassical plasma pedestal in a tokamak geometry *Phys. Plasmas* **11** 2649–67
[20] Chang C.S. and Ku S. 2006 Particle simulation of neoclassical transport in the plasma edge *Contrib. Plasma Phys.* **46** 496–503
[21] Ku S., Chang C.S. and Diamond P.H. 2009 Full-f gyrokinetic particle simulation of centrally heated global ITG turbulence from magnetic axis to edge pedestal top in a realistic tokamak geometry *Nucl. Fusion* **49** 115021
[22] Chang C.S., Ku S., Diamond P.H., Lin Z., Parker S., Hahm T.S. and Samatova N. 2009 Compressed ion temperature gradient turbulence in diverted tokamak edge *Phys. Plasmas* **16** 056108
[23] Snyder P.B. *et al* 2009 Pedestal stability comparison and ITER pedestal prediction *Nucl. Fusion* **49** 085035
[24] Dickinson D., Roach C.M., Saarelma S., Scannell R., Kirk A. and Wilson H.R. 2012 Kinetic instabilities that limit β in the edge of a tokamak plasma: a picture of an H-mode pedestal *Phys. Rev. Lett.* **108** 135002
[25] Wan W., Parker S.E., Chen Y. and Yan Z. 2012 Global gyrokinetic simulation of tokamak edge pedestal instabilities *Phys. Rev. Lett.* **109** 185004
[26] Saarelma S., Hill P., Bottino A., Colyer G., Field A.R., McMillan B., Peeters A., Roach C.M. and The MAST Team 2012 Global gyrokinetic turbulence simulations of MAST plasmas *Plasma Phys. Control. Fusion* **54** 085012
[27] Hatch D.R., Kotschenreuther M., Mahajan S., Valanju P. and Liu X. 2017 A gyrokinetic perspective on the JET-ILW pedestal *Nucl. Fusion* **57** 036020
[28] Lao L.L., John H.St., Stambaugh R.D., Kellmann A.G. and Pfeiffer W. 1985 Reconstruction of current profile parameters and plasma shapes in tokamaks *Nucl. Fusion* **25** 1611
[29] Parker S.E., Procassini R.J., Birdsall C.K. and Cohen B.I. 1993 A suitable boundary condition for bounded plasma simulation without sheath resolution *J. Comput. Phys.* **104** 41–9
[30] Yoon E.S. and Chang C.S. 2014 A Fokker–Planck–Landau collision equation solver on two-dimensional velocity grid and its application to particle-in-cell simulation *Phys. Plasmas* **21** 032503
[31] Hager R., Yoon E.S., Ku S., D'Azevedo E.F., Worley P.H. and Chang C.S. 2016 A fully non-linear multi-species Fokker–Planck–Landau collision operator for simulation of fusion plasma *J. Comput. Phys.* **315** 664

[32] Stotler D.P. and Karney C.F.F. 1994 Neutral transport modeling with DEGAS 2 *Contrib. Plasma Phys.* **34** 392–7
[33] Stotler D.P., Chang C.S., Park G. and Ku S.H. 2013 Energy conservation tests of a coupled kinetic–kinetic plasma-neutral transport code *Comput. Sci. Discovery* **6** 015006
[34] Battaglia D.J., Burrell K.H., Chang C.S., Ku S., deGrassie J.S. and Grierson B.A. 2014 Kinetic neoclassical transport in the H-mode pedestal *Phys. Plasmas* **21** 072508
[35] Krstic P.S. and Schultz D.R. 1998 Elastic and related transport cross sections for collisions among isotopomers of $H^+ + H$, $H^+ + H_2$, $H^+ + He$, and $H + H_2$ *At. Plasma-Mater. Data Fusion* **8** 1 (supplement to the *J. Nucl. Fusion*)
[36] Owen L.W., Colchin R.J., Maingi R., Fenstermacher M.E., Carlstrom T.N. and Groebner R.J. 2001 Origins and spatial distributions of core fueling in the DIII-D tokamak *J. Nucl. Mater.* **290–3** 464–8
[37] Horton W. 1999 Drift waves and transport *Rev. Mod. Phys.* **71** 735–78
[38] Diamond P.H., Itoh S.-I., Itoh K. and Hahm T.S. 2005 Zonal flows in plasma—a review *Plasma Phys. Control. Fusion* **47** R35–161
[39] Estrada T., Hidalgo C., Happel T. and Diamond P.H. 2011 Spatiotemporal structure of the interaction between turbulence and flows at the L-H transition in a toroidal plasma *Phys. Rev. Lett.* **107** 245004
[40] Hahm T.S., Na D.H., Lee J.W., Na Y.S., Kim S.S., Ko W.H., Diamond P.H., Jhang H. and Jeon Y.M. 2013 $E \times B$ shear suppression of turbulence in diverted H-mode plasmas: role of edge magnetic shear *Nucl. Fusion* **53** 093005
[41] Xu G.S. *et al* 2011 First evidence of the role of zonal flows for the L-H transition at marginal input power in the EAST tokamak *Phys. Rev. Lett.* **107** 125001